# Experimental Validation of a Nonlinear Wave Encounter Frequency Estimator Onboard a Wave-Propelled USV

**Alberto Dallolio** * **Jo A. Alfredsen** * **Thor I. Fossen** *
**Tor A. Johansen** *

* *Centre for Autonomous Marine Operations and Systems*
*Department of Engineering Cybernetics*
*Norwegian University of Science and Technology, Trondheim, Norway.*

**Abstract:** Knowledge of the amplitude and frequency of sea waves is useful to characterize the sea state, and increases the situational awareness as perceived by unmanned marine crafts. The ability to adapt navigation control parameters according to the current sea state is an essential feature for vehicles whose motion is mainly governed by environmental forces. From a control perspective, an estimate of the wave encounter frequency (WEF) can be used to filter out first-order wave-induced motions that cause undesired rudder control action and servo wear and deterioration. In this work we consider a nonlinear second-order observer capable of computing the approximate frequency of a sinusoidal signal with unknown amplitude and phase. This work presents the first experimental validation of the nonlinear estimator, which is tested for the first time on a five meters long wave-propelled unmanned surface vehicle (USV). Moreover, this article shows the estimator's ability to characterize the dominant frequency of wave spectra across different sea states and discusses two applications of the WEF estimation: sea state estimation and wave-filtered steering control. Theoretical considerations are supported with both simulation and experimental results.

*Keywords:* Maritime robotics; Guidance, navigation and control (GNC) of unmanned marine vehicles (surface and underwater); Autonomous and remotely operated marine vessels

## 1. INTRODUCTION

Sea state estimation is of importance in marine operations. It provides information that can be used to increase mission safety and reduce operational risk, but also to enhance the seakeeping and autopilot system performance of marine crafts whose motion is determined by sea waves, ocean currents and winds. Estimation of the WEF can be used to forewarn incoming impetuous waves and rough environmental conditions.

For autonomous vehicles whose propulsion and course-keeping capabilities mainly rely on environmental forces (Johnston and Poole, 2017; Hine et al., 2009; L3-Technologies, 2019), the estimation of the encounter frequency is relevant for two main reasons. First, it allows the vehicle to have in-situ situational awareness of the operational environment. Decision-making methods may benefit from estimates of the sea state and synthesize high-level mission plans that comply with the current condition of the environment. Moreover, by combining onboard estimates with meto-cean models it is possible to predict future sea states and eventually re-plan or modify the mission accordingly. Secondly, the estimated encounter frequency can be used as cut-off frequency in filters employed in wave filtering techniques for the rudder control command in a course-keeping controller (Fossen, 2021).

Spectral analysis is a commonly adopted technique used to study irregular waves and approximate them to a series of sinusoidal components with different amplitude, frequency and phase. This operation is commonly achieved by the Fast Fourier Transform (FFT) algorithm, that applies the Discrete Fourier Transform (DFT) on a window moving over the signal. This makes the transformation itself affected by lag and the estimation of the time-varying WEF based on obsolete data. Rather than estimating the whole wave spectrum, the dominant frequency could be observed instead and used for wave filtering. In addition, more accurate techniques allow to estimate the direction of incoming waves (Nielsen, 2006; Tannuri et al., 2003). However, these are constrained by the same lag affecting FFT and require a dynamic model of the vehicle, which in this case is complicated to derive due to the wave-propulsion assembly.

The signal-based method employed in this work is based on Belleter et al. (2013), where it is demonstrated that roll and pitch angles can be used to estimate the WEF. This approach was further extended to include a variation of the estimation algorithm that employs the heave displacement measured onboard the vehicle (Belleter et al., 2015). The same work, where the observer is tested on a container ship whose model and hydrodynamic coefficients can be found in Holden et al. (2007), contains the only experimental data prior to the present manuscript.

This article describes the validation of the WEF estimator on data collected by a wave-propelled USV (Dallolio et al., 2019). The algorithm is validated with simulations

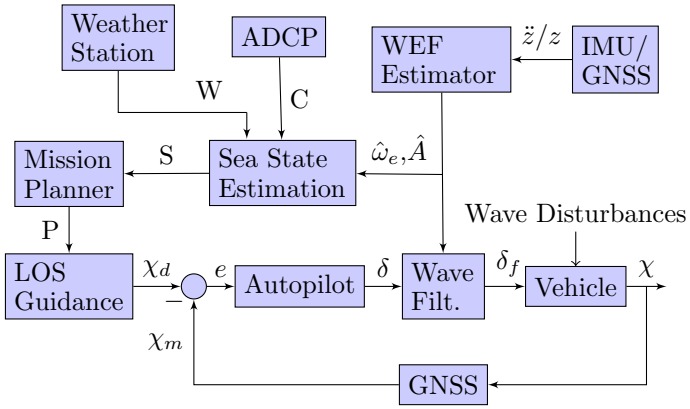


Fig. 1. Sea state estimation supports high-level mission planning and the GNC system onboard the USV.

and experimental results in both fjord and ocean waters, proving its ability to converge in different sea states.
The originality of this work stands in the application of a WEF observer to a small (5 meters long) USV, which shows completely different wave response and motion than a large ship, and which is never demonstrated before to the best of our knowledge. Moreover, the paper presents the first closed-loop field experiments employing this observer in a course-control architecture.

## 2. SEA STATE ESTIMATION & WAVE FILTERING ONBOARD WAVE-PROPELLED USV

The USV considered in this work is the AutoNaut [1] (Dallolio et al., 2019), a wave-propelled vehicle designed for persistent observation of the upper water column, achieved with a wide-range scientific payload sampling several water properties. The capability of performing long-endurance operations comes with challenges related to navigation, since the course and speed of the USV are mainly determined by environmental forces that, depending on the sea state, may prevail on the propulsion generated from waves. This motivates the need of a high-level entity capable of estimating the current sea state based on onboard sensor readings. Figure 1 indicates that, for example, sea currents ($C$) and surface winds ($W$) information can be merged, together with an estimate of the WEF ($\hat{\omega}_e$) and amplitude ($\hat{A}$), and used to estimate the current sea state ($S$). Moreover, onboard decision-making entities can evaluate the feasibility of the current mission and eventually modify or re-plan the intended mission (e.g. desired course change) to comply with the environment.
Figure 1 also indicates that the same estimated wave information can be employed in the onboard guidance, navigation and control (GNC) system for wave filtering of the rudder command signal. This article refers to wave filtering as the reduction of wave-induced control forces, that are a combination of second-order slowly varying and zero-mean first-order oscillatory components. Whereas the former can be canceled by an integral action, the latter may be removed from the measured motion states using a band-stop (or similar) filter. As discussed in Fossen (2021), precise knowledge of the encounter frequency allows better tuning of these filters. The figure indicates that filters for this purpose are usually placed between the autopilot and the vehicle servo, producing a filtered version ($\delta_f$) of the computed rudder angle ($\delta$) that reduces wear of the servo mechanism. It can also be configured to filter the course measurement before it is used for feedback control.

[1] http://autonaut.itk.ntnu.no/doku.php

## 3. HEAVE DYNAMIC MODEL

The heave motion of the USV can be modeled as a linear second-order system with sinusoidal forcing, Fossen (2021),

$$\ddot{z} + 2\zeta\omega_n\dot{z} + \omega_n^2 z = \frac{F}{m - Z_{\dot{w}}}\sin(\omega t + \varepsilon) \tag{1}$$

where $\omega$ is the modal (dominating) frequency of the waves, $z$ is the heave position, $\omega_n$ in the natural frequency, $\zeta$ is relative damping ratio, $F/(m - Z_{\dot{w}})$ is the wave force divided by mass (including hydrodynamic added mass $Z_{\dot{w}}$) and $\varepsilon$ is the oscillation phase. We only consider the steady-state solution

$$z = \frac{F}{(m - Z_{\dot{w}})Z_m\omega}\sin(\omega t + \varepsilon + \phi) \tag{2}$$

where $Z_m$ is the impedance or linear response function and $\phi$ is the phase angle relative to the driving force $F$. However, for a vehicle moving at ground speed $U > 0$, the Doppler Shift causes the wave angular frequency $\omega$ to be modified as

$$\omega_e(U, \omega, \beta) = \omega - kU\cos(\beta) \tag{3}$$

where $\omega_e$ is the *wave encounter frequency* (WEF), $k$ is the wave number satisfying the deep water dispersion relation $\omega^2 = kg$ in which $g$ is the acceleration of gravity and $\beta$ is the wave encounter angle (zero for following seas). The wave number $k$ relates to the wave length $\lambda$ as $k = 2\pi/\lambda$. This implies that the solution (2) can be reformulated as

$$z = A\sin(\omega_e t + \epsilon) \tag{4}$$

where

$$A = \frac{F}{(m - Z_{\dot{w}})Z_m\omega_e}, \quad \epsilon = \varepsilon + \phi \tag{5}$$

are the amplitude and phase of the measured heave position, respectively.

## 4. SWITCHING-GAIN WAVE ENCOUNTER FREQUENCY ESTIMATION

The estimation problem aims at estimating online the unknown frequency $\omega_e$ of a measured time-varying signal $z$ given by (4), whose amplitude $A$ and phase $\epsilon$ are not known. The sinusoidal signal (4) can be represented by the linear differential equation

$$\dddot{z} = \psi z \tag{6}$$

where $\psi := -\omega_e^2$ is the parameter to be estimated. As indicated in Aranovskiy and Bobtsov (2012), the frequency $\omega_e$ is estimated using the auxiliary filter

$$\begin{aligned} \dot{\zeta}_1 &= \zeta_2 \\ \dot{\zeta}_2 &= -2\omega_f\zeta_2 - \omega_f^2\zeta_1 + \omega_f^2 z. \end{aligned} \tag{7}$$

The filter cut-off frequency $\omega_f$ has to be chosen so that $0 < \omega_e < \omega_f$. The Laplace transformation of the linear system (7) leads to the transfer function

$$\zeta_1(s) = \frac{\omega_f^2}{(s + \omega_f)^2}z(s) \tag{8}$$

From (6) it follows that $s^2 z(s) = \psi z(s)$ and

$$z(s) = \frac{2\omega_f s + \omega_f^2 + \psi}{\omega_f^2}\zeta_1(s) \tag{9}$$

The time domain representation of (9) is recognized as

$$z = \frac{1}{\omega_f^2}\left(2\omega_f\zeta_2 + \omega_f^2\zeta_1 + \psi\zeta_1\right). \tag{10}$$

The parameter update law for $\psi$ presented in Aranovskii et al. (2007) makes use of the variable given by the auxiliary filter

$$z' := \dot{\zeta}_2 = -2\omega_f\zeta_2 - \omega_f^2\zeta_1 + \omega_f^2 z \tag{11}$$

By denoting $\hat{\psi}$ the parameter estimate and defining $\hat{z}' = \zeta_1\hat{\psi}$, the parameter update law becomes

$$\dot{\hat{\psi}} = k_f\zeta_1\left(\dot{\zeta}_2 - \zeta_1\hat{\psi}\right), \tag{12}$$

where $k_f$ is the adaptation gain obtained by low-pass filtering the gain switching mechanism as described in the next paragraph.
Global exponential stability of the equilibrium point of the estimator is proven in Belleter et al. (2015), where it is shown how the original fixed-gain estimation algorithm of Aranovskii et al. (2007) can be modified to include a gain adaptation algorithm, which depends on the estimated heave amplitude $\hat{A}$.

### *4.1 Switching-gain mechanism*

According to Belleter et al. (2013), we choose the switching mechanism for the gain as

$$k(A) = \begin{cases} k_{init} & \text{if } t \le t_{init} \\ k_{min} & \text{if } t > t_{init} \wedge A > A_0 \\ k_{max} & \text{if } t > t_{init} \wedge A \le A_0 \end{cases} \tag{13}$$

where $A$ is the signal amplitude, $A_0$ is the amplitude used to switch gains, and $t_{init}$ is the time duration in which the gain is in its initial value. The amplitude A of the measured signal cannot be directly computed. However, the amplitude can be estimated using the squared measurement

$$z^2 = \frac{A^2}{2}(1 - \cos(2\omega_e t + 2\epsilon). \tag{14}$$

Consequently, by low-pass filtering the signal (14), the amplitude $A^2/2$ of the squared measured signal $z^2$ is obtained

$$\gamma = \frac{1}{Ts+1}z^2, \tag{15}$$

where $T > 0$ implies that the estimate of amplitude becomes

$$\hat{A} = \sqrt{2\gamma}. \tag{16}$$

The adaptation gain $k_f(t)$ is obtained by low-pass filtering $k(\hat{A})$ according to

$$T_f\dot{k_f} + k_f = k(\hat{A}), \tag{17}$$

where $T_f > 0$ is recognized as the switching time constant and $k(\hat{A}) \le max(k_{max}, k_{init})$.

### *4.2 Preliminary considerations*

In this work we assume that the wave amplitude is similar to the heave amplitude of the USV (unitary transfer function in heave). Hence we use the heave amplitude measured by the GPS placed at the bow, after a transformation to the vehicle's BODY frame (located in the CG). The homogeneous transformation does not affect the measured heave period of the USV, but it uses the knowledge of lever arm and Euler angles to compute the heave in BODY frame, which shows intuitively a lower amplitude. For the purpose of WEF estimation, the effects of sensor location and lever arms can be neglected since it is primarily the time between peaks that contains information. Alternatively, it is possible to estimate the USV heave displacement from the vertical acceleration ($\ddot{z}$) measured by the IMU (Bryne et al., 2018), as indicated in Figure 1.
For wave periods in the interval $5 < T_w < 20$ seconds, the modal frequency $f$ of a wave spectrum will be in the range $0.05 < f < 0.2$ Hz. Therefore, the wave circular frequency $\omega = 2\pi f$ is in the range of $0.3 < \omega < 1.3$ rad/s. Fast and irregular waves are expected in fjords, where a reduced wind fetch generates short-crested waves whose amplitude and frequency are mainly dependent on the local wind speed. Typical fjord waves show therefore spectra with higher dominant frequencies $\omega > 1.3$ rad/s. Depending on the sea state, the measured speed over ground (SOG) of the USV may fluctuate between 0.5 and 2 knots (approximately 0.25 to 1 m/s). Figure 2 shows how the WEF, computed as in Equation (3), varies according to variations in waves encounter angle ($\beta$), vehicle ground speed ($U$) and wave frequency ($\omega$). As the wave direction and frequency are not directly measured, assumptions needs to be made according to weather forecasts.
The natural frequency of the USV heave motion is computed using standard methods from hydrostatics (Fossen, 2021). Assume that the added mass $-Z_{\dot{w}} = m$. Hence,

$$\omega_n = \sqrt{\frac{\rho g A_{wp}}{2m}}, \tag{18}$$

where $A_{wp}$ is the waterplane area and $\rho$ is the seawater average density 1025 kg/m$^3$. An estimate of $\omega_n$ can be found by approximating the USV as a box for which $A_{wp} = LB$ (length times beam). Furthermore, the mass $m$ of a box-shaped USV is $m = \rho LBT_{USV}$ where $T_{USV}$ is the draught. Hence,

$$\omega_n \approx \sqrt{\frac{g}{2T_{USV}}}, \tag{19}$$

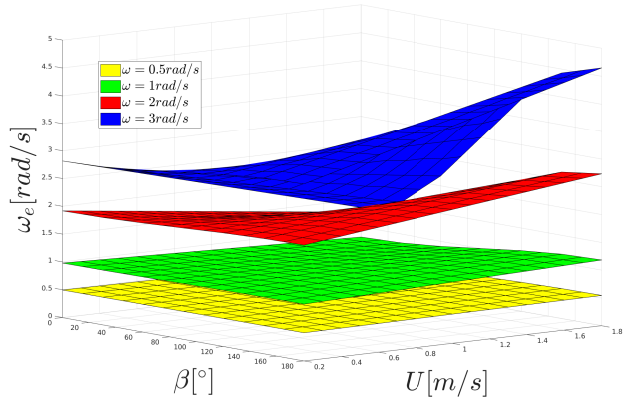


Fig. 2. Expected WEF perceived by the USV based on varying ground speed $U$, encounter angle $\beta$ and wave frequency $\omega$.

Table 1. Estimator Parameters

| Parameter | Symbol | Value |
|---|---|---|
| Switching time constant | $T_f$ | 0.05 s |
| Filter cut-off frequency | $\omega_f$ | 1.5 rad/s |
| Initial frequency | $\hat{\omega}_e^{init}$ | 0 rad/s |
| Switching amplitude | $A_0$ | 0.5 m |
| Initialization time | $t_{init}$ | 200 s |
| Adaptation gains (S1) | $k_f^{S1}$ | 10,5,25 |
| Adaptation gains (S2) | $k_f^{S2}$ | 25,10,50 |

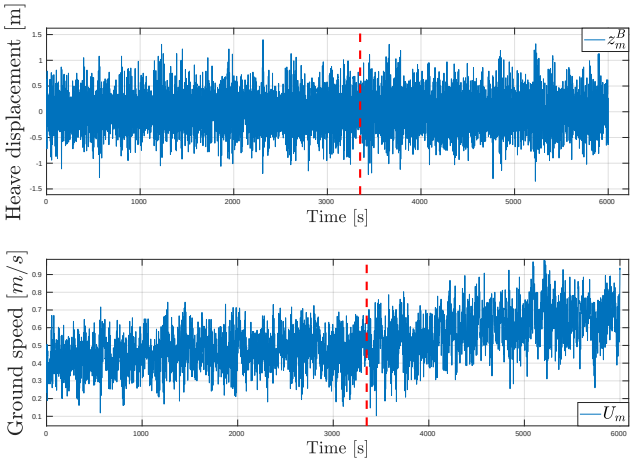


Fig. 3. Top: heave displacement ($z_m^B$). Bottom: USV ground speed ($U_m$).

The vehicle draft $T_{USV} = 0.3$ m (0.7 m including the submerged struts and hydrofoils) gives $\omega_n = 4.1$ rad/s, which corresponds to a heave period of approximately 1.5 seconds. Hence, the natural frequency is far away from the WEF and resonance situations are avoided.

## 5. OFFLINE EXPERIMENTAL VALIDATION

The estimated encounter frequency is compared to the dominant frequency observed with spectral analysis (FFT). Moreover, we compute and compare the average frequency of heave peaks measured by the GPS. This does not indicate the dominant frequency of the asymmetric wave spectrum and therefore we expect the frequency $\hat{\omega}_e$ estimated by the observer to be higher. Tables 1 and 2 contain the employed estimator parameters, where $\hat{\omega}_e^{init}$ is the initial WEF.

### *5.1 Experimental validation in the Norwegian Sea*

The estimation algorithm was first tested on data collected in the ocean, 40km north-west of the island Frøya situated along the coasts of Central Norway. We focus on a 100 minutes long portion of the collected data in which there is an increase of USV ground speed from 0.4 m/s to 0.7 m/s on average. The red dashed line in Figure 3 indicates the separation before and after the speed increase. The estimator is run with parameters indicated in Table 1. Figure 4 shows the WEF ($\hat{\omega}_e$) estimated with different sets of gains ($S1, S2$) and same initial value ($\hat{\omega}_e^{init}$) for the estimation. The estimation results are compared to the average frequencies ($\bar{\omega}_e^P$, yellow lines) obtained by computing local maxima of the heave signal ($z_m^B$ in Figure 3), on both trajectory legs. Local maxima are data samples that are

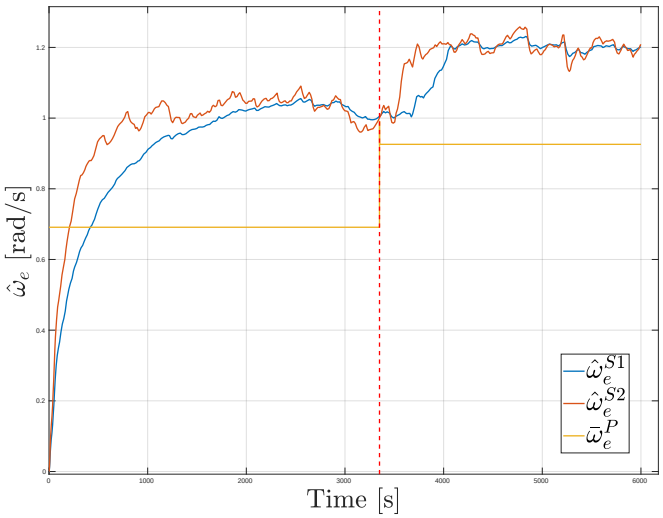


Fig. 4. Estimated WEF with different gains sets ($\hat{\omega}_e^{S1}$, $\hat{\omega}_e^{S2}$), as compared to average frequency computed from heave peaks ($\bar{\omega}_e^P$).

larger than its two neighboring samples. It can be noticed that the set of higher gains ($S2$) allows the estimator to converge faster ($\hat{\omega}_e^{S2}$) to approximately 1 rad/s and 1.2 rad/s and that the estimation trend resembles the average frequencies computed in each leg. Higher estimated values are however observed since the estimator extracts the peak in the spectrum. Ground truth is obtained with FFT spectral analysis (Figure 5), that reveals higher peaks around the estimated frequencies observed in Figure 4, and proves the ability of the observer to estimate dominant frequencies in both spectra.

### *5.2 Experimental validation in the Trondheim Fjord*

Figure 6 shows the heave measurement collected while the USV executed autonomously a squared trajectory in Trondheimsfjord. The estimator was run with parameters indicated in Table 2 and same sets of gains of Table 1. Figure 7 shows the estimated WEF for both gain sets and compares it to the average frequency measured from the

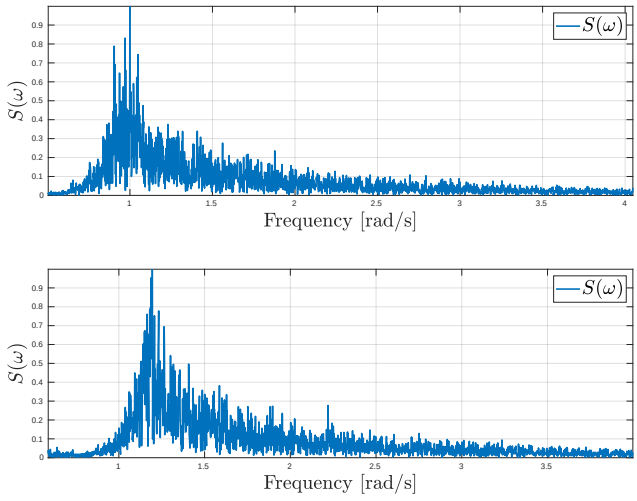


Fig. 5. FFT indicates the range of frequencies present in the heave signal $z_m^B$. Top: before wind speed increase. Bottom: after wind speed increase.

Table 2. Estimator Parameters

| Parameter | Symbol | Value |
|---|---|---|
| Switching time constant | $T_f$ | 0.05 s |
| Filter cut-off frequency | $\omega_f$ | 4 rad/s |
| Initial frequency | $\hat{\omega}_e^{init}$ | 2 rad/s |
| Switching amplitude | $A_0$ | 0.2 m |
| Initialization time | $t_{init}$ | 200 s |

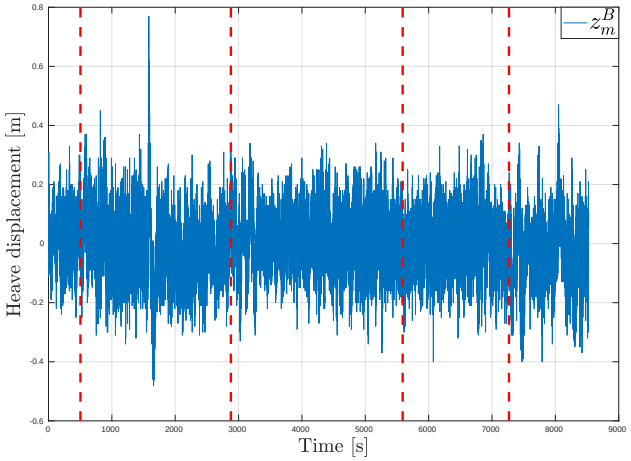


Fig. 6. Heave displacement in body frame ($z_m^B$); red dashed lines indicate change in desired course.

heave signal. Even if the convergence speed is increased by setting the initial frequency to 2 rad/s, it is observed that the amount of data collected in the first trajectory leg is not enough to achieve convergence. Again the use of a set of higher gains ($S2$) leads to a faster convergence.
FFT in Figure 8 shows richer spectra with frequencies in the range of 1.5 and 4 rad/s. It can be noticed that the frequencies at which the estimator converges (Figure 7) match, in each section of the trajectory, with the peaks observed in FFT spectral analysis. Moreover, wave spectra do not contain significant energy at lower frequencies, indicating predominance of irregular waves on swell components.

## 6. WAVE-FILTERED STEERING CONTROL

The estimator was implemented on the USV onboard navigation software DUNE (Pinto et al., 2012) and tested during open ocean operations. The observer ran at regular

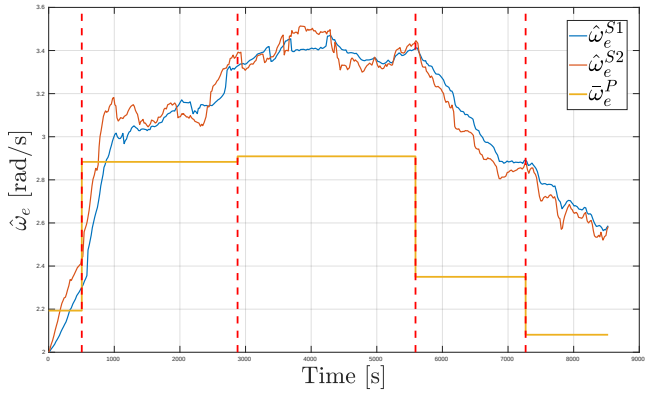


Fig. 7. Estimated WEF with different gains sets ($\hat{\omega}_e^{S1}$, $\hat{\omega}_e^{S2}$), as compared to average frequency computed from heave peaks ($\bar{\omega}_e^P$).

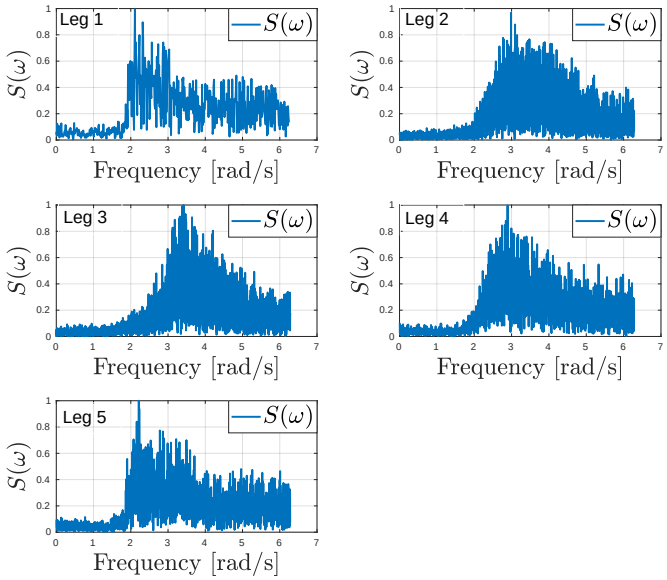


Fig. 8. FFT spectral analysis indicates the range of frequencies present in the heave signal $z_m^B$, for each trajectory section.

time intervals with initial frequency $\hat{\omega}_e^{init}$ obtained from the previous run. Once estimation stabilized to a range of values, the estimated WEF was used to filter the rudder angle signal computed by the course autopilot as shown in Figure 1. The course-keeping autopilot used in this mission is a PI controller with gains $K_p = 1$ and $K_i = 0.1$. Wave filtering is achieved with a first-order low-pass filter with cut-off frequency $\omega_{LP} = n\hat{\omega}_e$ where $n = 1.2$ is chosen in order to remove only high-frequency components. The filter cut-off frequency is computed from an estimated WEF $\hat{\omega}_e = 1.12$ rad/s. Figure 9 compares magnitude and phase of the closed-loop transfer functions (from course reference to course) with and without the filter, $H_{LP}(s)$ and $H(s)$ respectively. This analysis assumes that the USV's steering dynamics is represented by a first-order

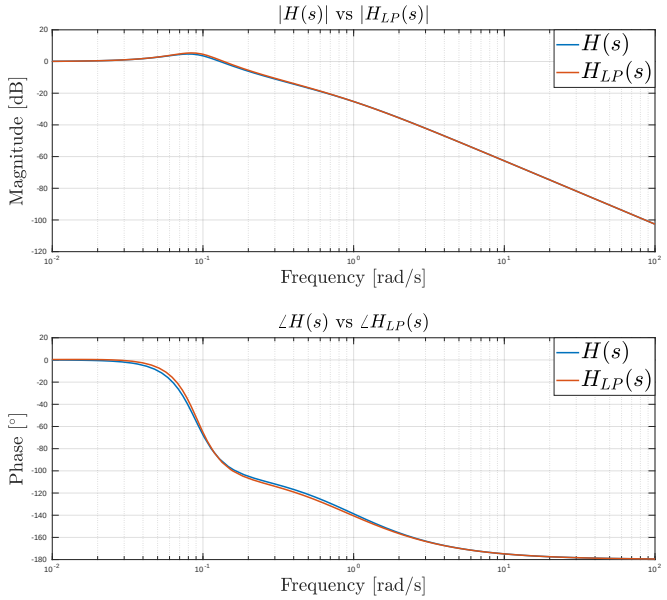


Fig. 9. Bode plots of the closed loop transfer functions with ($H_{LP}(s)$) and without ($H(s)$) low-pass filter.

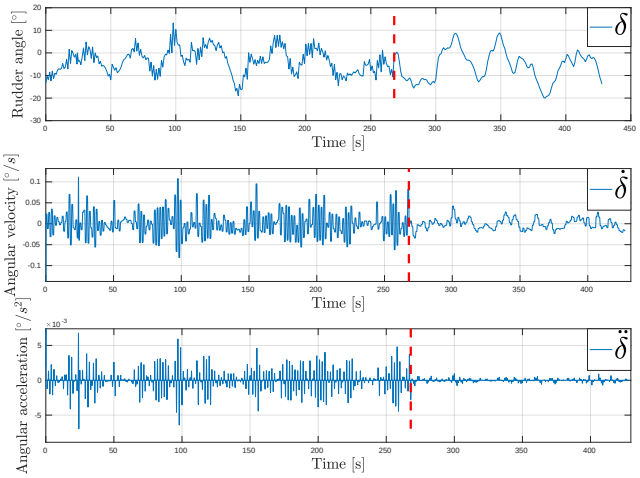


Fig. 10. Commanded rudder angle $\delta$ (top) and its derivatives $\dot{\delta}$ (middle) and $\ddot{\delta}$ (bottom).

Nomoto model (Fossen, 2021) with parameters identified in Agdal (2018). It can be observed that the systems show the same response at high frequencies and a negligible difference up to 2 dB in magnitude and 4° in phase at low frequencies.

Figure 10 shows the rudder response when the low-pass filter is applied at time $t = 265$ s (red dashed line). The suppression of high frequencies is clear, despite the amplitude of rudder oscillations (bounded to approximately 10°) is not affected. This indicates that the control bandwidth of the system was not significantly reduced (as the Bode plot confirms) and that despite the suppression of undesired wave-induced frequencies the autopilot is still able to command large oscillations to adjust the USV's course. While the rudder angle ($\delta$) is logged onboard the USV, angular velocity ($\dot{\delta}$) and acceleration ($\ddot{\delta}$) are obtained offline. Figure 10 shows that the amplitude of the rudder angle velocity oscillations reduces of approximately 61% after the application of the filter. This increases the mechanism lifetime since prolonged use of the rudder at higher angular velocities is what wears the servo mechanism the most. Angular acceleration oscillations are instead damped by 89% of their average value when the filter is introduced, also limiting rudder jerks and therefore the stress on the mechanism. From a course-control perspective, Figure 11 shows that course-keeping performance is not impacted once the filter is introduced in the control loop, since similar course oscillations (with amplitude within 15°) are observed before and after the application of the rudder signal filter at time $t = 265$ s.

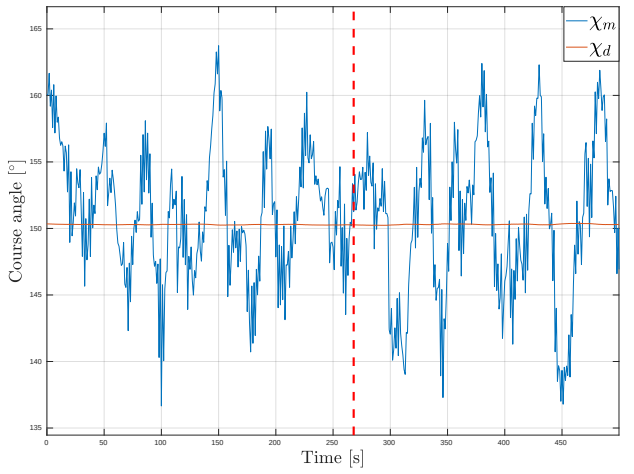


Fig. 11. Measured ($\chi_m$) and desired ($\chi_d$) course over ground, before and after filtering (red dashed line).

## 7. CONCLUSION

In this article we discuss the validation of a nonlinear WEF estimator, which is tested on experimental data collected by a 5 meters long wave-propelled USV during field campaigns in the fjord and in the ocean. The estimated WEF is compared to the dominant frequency obtained with FFT, used as ground truth, and to the average frequency observed in the USV's heave measurement. Offline experimental results prove the ability of the observer to identify the dominant frequency in different waves spectra (ocean and fjord). Online use of the estimator onboard the USV is shown and experimental results clearly indicate the benefits of using the discussed algorithm for wave filtering of the rudder command from the course-keeping autopilot. The obtained results show the benefits of using the WEF estimator for the computation of the dominant frequency of wave encounters, due to its lower computational needs as compared to FFT and search for local maxima in the heave measurement. Moreover, the use of the estimated WEF for wave filtering of the rudder command implies a significant suppression of the USV's rudder motions at higher frequencies. However, this does not involve an amplitude reduction in the rudder's commanded angles, allowing the onboard controller to maintain course-keeping performance. On the other hand, significant reduction of wave-induced motions of the servo reduces wear and stress while increasing the mechanism lifetime.

Sustained autonomous control is still an open challenge and even more so under the highly dynamic environmental changes experienced by an USV. Commanded and generated plans would likely be invalid during sustained exploration, relying on shore-based operators for support with new or modified mission goals. This, together with the fact that communication with shore could be sporadic and costly over expensive satellite links, motivates the need for the system to be self aware, robust to operational risks and failures, and therefore capable to generate its own goals. In this article we indicate how the estimated WEF can additionally be used onboard a small USV to increase its situational awareness about the environment, by merging this knowledge with onboard sensors measurements and eventually re-planning the USV's intended route.

## ACKNOWLEDGEMENTS

This work was supported by the Research Council of Norway (RCN) through the MASSIVE project, grant number 270959, and the center of excellence (AMOS) grant number 223254. The authors would like to thank Pedro De La Torre for the support with the operations and logistics, and Torleiv Bryne and Henning Øveraas for the precious comments.

Agdal, B.O. (2018). *Design and Implementation of Control System for Green Unmanned Surface Vehicle*. Master's thesis, NTNU.

Aranovskii, S.V., Bobtsov, A.A., Kremlev, A.S., and Luk'yanova, G.V. (2007). A robust algorithm for identification of the frequency of a sinusoidal signal. *Journal of Computer and Systems Sciences International*, 46(3), 371–376. doi:10.1134/S1064230707030045. URL `https://doi.org/10.1134/S1064230707030045`.

Aranovskiy, S. and Bobtsov, A. (2012). Output harmonic disturbance compensation for nonlinear plant. In *2012 20th Mediterranean Conference on Control Automation (MED)*, 386–391. doi:10.1109/MED.2012.6265668.

Belleter, D.J., Breu, D.A., Fossen, T.I., and Nijmeijer, H. (2013). A globally k-exponentially stable nonlinear observer for the wave encounter frequency. *IFAC Proceedings Volumes*, 46(33), 209 – 214. doi:https://doi.org/10.3182/20130918-4-JP-3022.00016. 9th IFAC Conference on Control Applications in Marine Systems.

Belleter, D.J., Galeazzi, R., and Fossen, T.I. (2015). Experimental verification of a global exponential stable nonlinear wave encounter frequency estimator. *Ocean Engineering*, 97, 48 – 56. doi:https://doi.org/10.1016/j.oceaneng.2014.12.030.

Bryne, T., Rogne, R., Fossen, T., and Johansen, T. (2018). A virtual vertical reference concept for aided inertial navigation at the sea surface. *Control Engineering Practice*, 70, 1–14. doi:10.1016/j.conengprac.2017.09.009.

Dallolio, A., Agdal, B., Zolich, A., Alfredsen, J.A., and Johansen, T.A. (2019). Long-endurance green energy autonomous surface vehicle control architecture.

Fossen, T. (2021). *Handbook of Marine Craft Hydrodynamics and Motion Control, 2n Edition*. Wiley. doi:10.1002/9781119994138.

Hine, R., Willcox, S., Hine, G., and Richardson, T. (2009). The wave glider: A wave-powered autonomous marine vehicle. In *OCEANS 2009*, 1–6. doi:10.23919/OCEANS.2009.5422129.

Holden, C., Galeazzi, R., Rodríguez, C., Perez, T., Fossen, T.I., Blanke, M., de Almeida, M., and Neves, S. (2007). Nonlinear Container Ship Model for the Study of Parametric Roll Resonance. *Modeling, Identification and Control*, 28(4), 87–103. doi:10.4173/mic.2007.4.1.

Johnston, P. and Poole, M. (2017). Marine surveillance capabilities of the autonaut wave-propelled unmanned surface vessel (usv). In *OCEANS 2017 - Aberdeen*, 1–46. doi:10.1109/OCEANSE.2017.8084782.

L3-Technologies (2019). C-enduro long endurance ASV.

Nielsen, U. (2006). Estimations of on-site directional wave spectra from measured ship responses. *Marine Structures*, 19, 33–69. doi:10.1016/j.marstruc.2006.06.001.

Pinto, J., Calado, P., Braga, J., Dias, P., Martins, R., Marques, E., and Sousa, J. (2012). Implementation of a control architecture for networked vehicle systems. *IFAC Proceedings Volumes*, 45(5), 100 – 105. doi:https://doi.org/10.3182/20120410-3-PT-4028.00018. 3rd IFAC Workshop on Navigation, Guidance and Control of Underwater Vehicles.

Tannuri, E., V. Sparano, J., N. Simos, A., and J. Da Cruz, J. (2003). Estimating directional wave spectrum based on stationary ship motion measurements. *Applied Ocean Research*, 25, 243–261. doi:10.1016/j.apor.2004.01.003.